Acoustic charge transport in GaN nanowires

J. Ebbecke, S. Maisch, Achim Wixforth, R. Calarco, R. Meijers, M. Marso, H. Lüth

Angaben zur Veröffentlichung / Publication details:

Ebbecke, J., S. Maisch, Achim Wixforth, R. Calarco, R. Meijers, M. Marso, and H. Lüth. 2008. "Acoustic charge transport in GaN nanowires." *Nanotechnology* 19 (27): 275708. https://doi.org/10.1088/0957-4484/19/27/275708.

Acoustic charge transport in GaN nanowires

J Ebbecke[1,2], S Maisch[1], A Wixforth[1], R Calarco[3], R Meijers[3], M Marso[3] and H Lüth[3]

[1] Experimentalphysik I, Institut für Physik der Universität Augsburg, Universitätsstraße 1, 86135 Augsburg, Germany
[2] School of Engineering and Physical Sciences, Heriot-Watt University, Edinburgh, EH14 4AS, UK
[3] Institute of Bio- and Nanosystems (IBN1) and cni—Center of Nanoelectronic Systems for Information Technology, Research Centre Jülich, 52425 Jülich, Germany

Abstract

We present acoustic charge transport in GaN nanowires (GaN NWs). The GaN NWs were grown by molecular beam epitaxy (MBE) on silicon(111) substrates. The nanowires were removed from the silicon substrate, aligned using surface acoustic waves (SAWs) on the piezoelectric substrate $LiNbO_3$ and finally contacted by electron beam lithography. Then, a SAW was used to create an acoustoelectric current in the GaN NWs which was detected as a function of radio-frequency (RF) wave frequency and its power. The presented method and our experimental findings open up a route towards new acoustic charge transport nanostructure devices in a wide bandgap material such as GaN.

(Some figures in this article are in colour only in the electronic version)

1. Introduction

Self-organized structures using 'bottom up' approaches are expected to play an important role in future nanoelectronics. There exists intense research involving self-organized one-dimensional structures like carbon nanotubes and semiconductor nanowires. Many different device structures such as resonant tunnelling diodes (RTDs) (Björk *et al* 2002), single electron transistors (SETs) (Thelander *et al* 2003), field effect transistors (Greytak *et al* 2004), and biosensors (Zhong *et al* 2003) based on NWs have been reported already, but still many fundamental questions remain unanswered up to now.

GaN as a wide bandgap semiconductor is a promising candidate for novel NW devices. Therefore, a large interest in the scientific community has been devoted to study the electronic and optoelectronic properties of self-organized GaN wires (Calarco *et al* 2005, Huang *et al* 2002, Hwang *et al* 2004, Cavallini *et al* 2006, Motayed *et al* 2006, Cavallini *et al* 2007).

Since the invention of acoustic charge transport (ACT) devices in GaAs (Hoskins *et al* 1982) there has been an increasing interest driven by applications in analogue signal processing. In ACT devices, the dynamic piezoelectric potential of a propagating surface acoustic wave is able to convey charges in the wave propagation direction. Favoured by the slower velocity of the acoustic wave compared with the speed of light, and also because of the possibility to transmit information analogically, there are many applications, such as for example delay lines and high-speed monolithic signal processors (Hoskins *et al* 1982, Schmukler and Hoskins 1988, Rotter *et al* 1999), that can be successfully implemented.

Surface acoustic waves (SAWs), typically excited by means of so-called interdigital transducers, can be regarded as quasi-monochromatic acoustic phonons with a well-defined wavevector. Typical frequencies are in the several hundred MHz regime, the mechanical amplitudes are typically below 1 nm, and the corresponding wavelengths are a few microns. The absorption of acoustic phonons in an electronic system results in an acoustoelectric current. The acoustoelectric current density j in macroscopic systems is known to obey the well-known Weinreich relation (Weinreich 1956):

$$j = \mu \frac{\Gamma S}{w}.$$

Here μ denotes the charge carrier mobility, Γ is the acoustic absorption coefficient, S the acoustic intensity and w the sound velocity. However, in quantum systems this relation needs to be modified (Shilton *et al* 1996, Gurevich *et al* 1998, Rotter *et al* 1998).

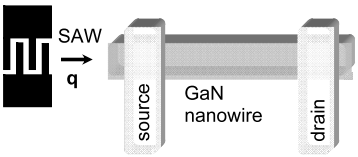

Figure 1. Sketch of sample layout under investigation. A GaN nanowire is contacted with source and drain electrodes and a SAW induces an acoustoelectric current in the system.

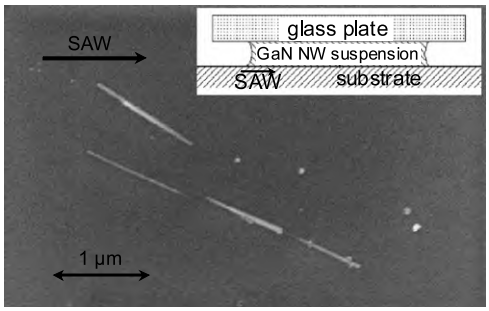

Figure 2. SEM picture of SAW-aligned GaN nanowires. The experimental setup with one drop of nanowire suspension placed in the cavity between the $LiNbO_3$ substrate and a glass plate is shown as an inset.

In this paper, ACT devices using self-organized GaN wires are presented. A schematic sketch of the system under consideration is presented in figure 1. A GaN NW is contacted with source and drain electrodes, and a SAW with wavevector **q** and a propagation direction parallel to the length of the wire is launched. The interaction of the acoustic phonons and charge carriers (for example by absorption of ultrasonic phonons) is supposed to create a net drag of the charge carriers and hence a DC acoustoelectric current. The investigation of SAW induced acoustoelectric current in GaN NWs is the main focus of this paper. Additionally, we will discuss to what extent the ACT in GaN NWs can be described by the Weinreich relation.

2. Preparation of GaN nanowire samples

Self-assembled GaN NWs are grown by radio-frequency (RF) plasma-assisted molecular beam epitaxy (MBE) on Si(111) substrates under nitrogen rich (III/V ratio $\ll 1$) conditions at 780 °C, which leads to the desired columnar growth in the c-direction. The details of the fabrication process can be found elsewhere (Meijers 2006). After epitaxial growth, NWs were released from the native Si(111) substrate by exposure to an ultrasonic bath of deionized water with a few milligrammes of sodium dodecylsulfate (SDS). Then, the wires were deposited on a host substrate. SDS is used to enhance the dispersion of the GaN NWs.

Two types of sample (A and B) will be discussed in this paper: the difference between the samples is the piezoelectric host material. Sample A employs a standard single-crystal $LiNbO_3$ substrate (rotation 128°, Y-cut, X-propagation) with a conductivity of $10^{-18}\ \Omega^{-1}\ \mathrm{cm}^{-1}$; it is piezoelectric and also pyroelectric. The substrate of sample B is so-called black $LiNbO_3$ (rotation 128°, Y-cut, X-propagation) which has been chemically reduced to a conductivity $>10^{-11}\ \Omega^{-1}\ \mathrm{cm}^{-1}$ (Bordui *et al* 1999). In this case, its piezoelectricity is basically the same as in the case of sample A, but due to the higher conductivity the black $LiNbO_3$ is less pyroelectric.

3. Parallel fluidic organization of nanowires

On sample A, an interdigital transducer (IDT_1) was processed by optical lithography. The IDT_1 periodicity p_1 is 32 μm. Using the value of 3840 m s^{-1} for the SAW velocity w, the resonance frequency $f_1 = w/p$ of the IDT_1 results to be $f_1 = 120$ MHz. A single droplet of SDS suspension containing GaN NWs was placed on sample A next to the IDT_1 and then covered with a glass plate (see the inset of figure 2). An RF power of $P = 17$ dBm at the resonance frequency $f = f_1$ was applied to IDT_1, resulting in a SAW with large amplitude. As presented in earlier work for multi- or single-walled metallic carbon nanotubes (Strobl *et al* 2004), the travelling piezoelectric SAW potential induces a dipole force in long wires that has an alignment effect parallel to the SAW propagation direction. Moreover, the SAW on the present $LiNbO_3$ substrate cut is a Rayleigh wave. This also involves a movement of the atoms that are near the surface in the vertical direction. These movements can lead to an acoustic streaming in a liquid and it has been shown in Strobl *et al* (2004) that the superposition of the liquid streaming effect and the induced dipole forces results in an alignment at a finite angle to the wave propagation direction. A similar aligning effect of SAWs for GaN NWs is found in the present work, as presented in figure 2, but less pronounced than for the carbon nanotubes. Here, only GaN NWs longer than 1 μm are aligned with respect to the SAW direction. The reduced alignment effect can be attributed to the lower conductivity of the nominally undoped semiconducting GaN NWs as compared to metallic carbon nanotubes.

4. Sample preparation on $LiNbO_3$

After GaN NW deposition and alignment, sample A was covered with a conductive polymer under which the position of a single GaN NW with respect to prestructured markers was located employing a scanning electron microscope (SEM). The polymer was removed afterwards in an oxygen plasma and the sample was covered with a double layer of PMMA and a 25 nm thick layer of aluminium. The thin layer of aluminium ensured a finite sample surface conductivity for electron beam lithography without severely influencing the electron beam exposure process. After writing the contact structures the aluminium was removed in diluted KOH. Finally, metal contacts (20 nm Ti and 30 nm Au) were deposited and patterned by a lift-off process. An SEM image of the central part of sample A (obtained after measurements) with source, drain and gate contacts is shown in figure 3(a). The length of the GaN NW between the contacts is approximately 1 μm, with a whole wire length of approximately 2 μm and a wire diameter of 160 nm.

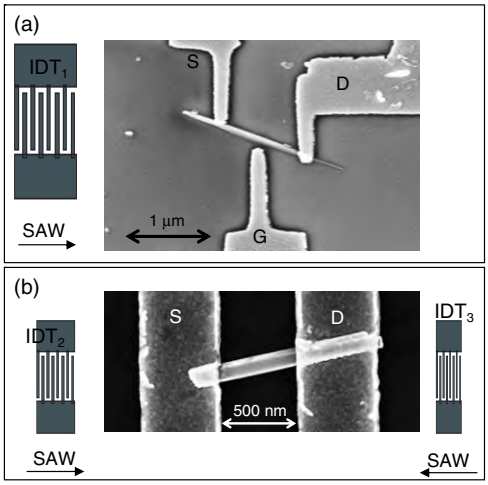

Figure 3. SEM image of the sample structure. (a) Sample A: GaN NW on standard $LiNbO_3$ with source, drain and gate electrodes. The SAW propagation direction is indicated. (b) Sample B: GaN NW on black $LiNbO_3$ with source and drain contacts; here, SAWs with different wavelengths can be excited from both sides of the NW.

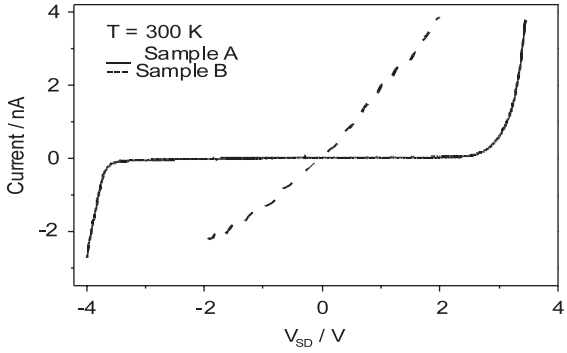

Figure 4. Current–voltage characteristics of the contacted GaN NW. Sample A exhibits a strong nonlinear dependence whereas the contacts of sample B exhibit a much better ohmic characteristic.

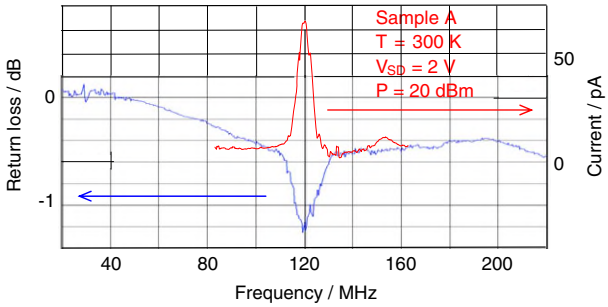

Figure 5. DC acoustoelectric current as a function of RF frequency in the GaN NW: return loss S11 measurement at IDT_1 of sample A. At the same frequency (the IDT_1 resonance frequency) a current signal was detected while launching a SAW with an RF power of $P = 20$ dBm.

For sample B, due to the higher conductivity of the black $LiNbO_3$, it was possible to use a standard electron beam lithography technique. After applying the fluidic alignment process described before, pairs of source drain fingers were randomly deposited by electron beam lithography and oriented perpendicularly to the alignment direction. High frequency interdigital transducers IDT_2 and IDT_3 were processed at the same time with a periodicity $p_2 = 3.6$ μm and $p_3 = 2$ μm. Afterwards, the substrate was inspected with an SEM and only finger pairs being bridged by a single GaN NW were chosen for further investigation. One of these contacted structures is shown in figure 3(b). The length of the contacted GaN NW in this case is approximately 500 nm, with a whole wire length of approximately 1.3 μm and a wire diameter of 110 nm.

5. Electrical properties of GaN nanowires

First, conventional current–voltage (I–V) measurements were made to characterize the contacted single GaN NW devices. In figure 4, a comparison of the I–V characteristic of sample A and sample B is shown. For sample A, a bias of at least $V_b = 3$ V needs to be applied to the contacts to measure a significant current. Similar characteristics were found for many different contacted GaN NWs on this substrate. We assume this to be caused by imperfect contacts between the GaN NWs on standard $LiNbO_3$. The deposition and removal of the conductive polymer for SEM inspection during the sample preparation (see section 4) or/and the strong piezoelectric fields caused by the pyroelectric effect during processing might be the reasons for the bad contacts. This assumption is also based on the fact that the contacts to GaN NWs of the same MBE growth nanowire batch on the second substrate material (black $LiNbO_3$) were found to show much better ohmic behaviour. One example of an I–V characteristic for sample B is shown in figure 4 (dashed line). This I–V curve exhibits a much higher conductance compared to sample A, and is in qualitative agreement with previously published results on GaN single NW devices on Si/SiO_2 samples (Calarco *et al* 2005).

6. Frequency dependence of acoustoelectric current

The return loss S11 of the IDT_1 of sample A is shown in figure 5. S11 was measured with a network analyser and shows a resonance at $f_1 = 120$ MHz in good agreement with periodicity $p_1 = 32$ μm. At the same frequency, the DC current through the wire has a peak value, as can be seen in figure 5. Here, the DC current through the GaN NW was measured as a function of the RF frequency applied to the IDT. A relatively high power RF signal of $P_1 = 20$ dBm was applied to the IDT_1. To measure a finite acoustoelectric current, an additional DC source–drain voltage of $V_{SD} = 2$ V needed to be applied. In spite of this, the coincidence of the resonant frequencies in S11 and the current as shown in figure 5 prove the current to be caused by the presence of the SAW. Therefore, the launching of a SAW by applying a resonant RF signal to the IDTs results in a DC acoustoelectric current in the GaN NW.

Due to the much better defined contacts on GaN NW sample B, here, an acoustoelectric current could be detected without the need for an additional source–drain voltage. This acoustoelectric current as a function of applied RF frequency is shown in figure 6. Two IDTs with different periodicities

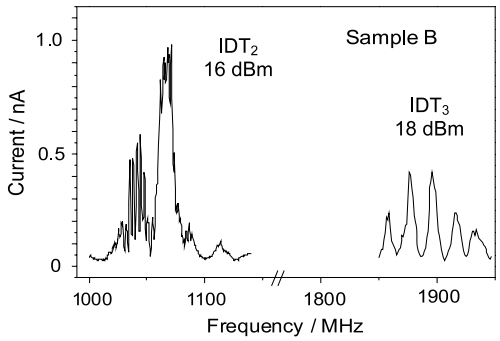

Figure 6. Acoustoelectric current at zero source–drain voltage for sample B being solely induced by the SAWs excited at the two IDTs with a periodicity of $p_2 = 3.6\ \mu$m and $p_3 = 2\ \mu$m. The current oscillations are caused by Bragg reflections of the SAW at unused spare IDTs (see text).

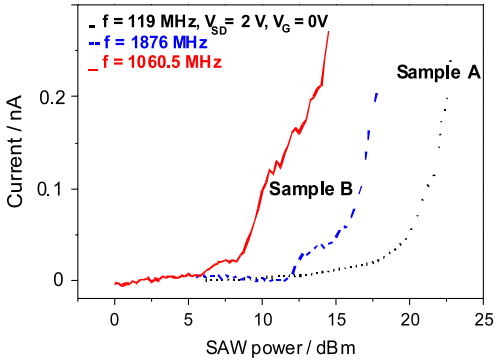

Figure 7. Acoustoelectric current in sample A and sample B as a function of RF power for different SAW frequencies. Apart from the monotonic DC current increase for sample A, there are non-monotonic features of the acoustoelectric current characteristics of sample B.

have been processed on either side of the GaN NW single device. The left IDT_2 (see figure 3(b)) has a periodicity of $p_2 = 3.6\ \mu$m and the right one a periodicity of $p_3 = 2\ \mu$m. The detected acoustoelectric current in this GaN NW of sample B exhibits two peaks at two frequencies $f_2 = 1070$ MHz and $f_3 = 1880$ MHz, as expected from $f = w/p$. Additionally, the current in figure 6 exhibits a superimposed oscillation pattern with a frequency of $f_{osc2} = 3.2$ MHz and $f_{osc3} = 19$ MHz. These oscillations have their origin in SAW reflections at about 0.6 mm to the left and about 0.1 mm to the right of the contacted GaN NW, respectively. The distances and hence the locations of the SAW reflectors are calculated using the formula distance$/2 = 3840\ \mathrm{m\,s^{-1}}/f_{osc}$. At these exact spots, additional IDTs with the same periodicity as IDT_2 and IDT_3 were present on the sample (not shown) acting as very efficient Bragg reflectors for the SAWs causing the current oscillations observed in figure 6. Between these reflectors, a Fabry–Perot type of resonator was formed, leading to the evolution of a standing wave pattern. Hence, the observed acoustoelectric current is caused by a propagating SAW with a superimposed standing wave of smaller amplitude (because the reflected amplitude is smaller than the original one). By changing the SAW frequency inside the IDT passband, the position of the knots and bellies of the superimposed standing wave is shifted with respect to the GaN NW, resulting in an oscillation of the induced acoustoelectric current. This phenomenon was detected in many semiconductor SAW devices where IDTs with the same periodicity were processed on either side of the semiconductor nanostructure (see for example Talyanskii *et al* 1997).

7. RF power dependence of acoustoelectric current

Finally, the acoustoelectric current was measured for fixed resonance frequencies f_1, f_2 and f_3 for the two samples as a function of the applied RF power. An increased RF power causes a larger SAW amplitude. These investigations are presented in figure 7. The SAW wavelength $\lambda_1 = 32\ \mu$m of sample A is much longer than the contacted region of the GaN NW. The acoustoelectric current of sample A as a function of RF power is presented as a dotted line in figure 7; it exhibits a monotonic increase of induced DC current for increased RF power, i.e. SAW amplitude. This dependence can be explained nicely with the Weinreich equation. A larger acoustic intensity S leads to an increased acoustoelectric current J. Please note that for this measurement an additional source–drain voltage of $V = 2$ V was applied, as in figure 5. In the case of sample B, the SAW, although at much higher frequencies than for sample A, also leads to a finite acoustoelectric current. The continuous and dashed lines in figure 7 surprisingly show a non-monotonic increase of the acoustoelectric currents. Such a non-monotonic increase of the acoustoelectric current cannot be explained easily with the Weinreich relation.

In Shilton *et al* (1996), the acoustoelectric current in an one-dimensional ballistic conductor was investigated and an oscillation of the acoustoelectric current was observed and explained. It was found that the magnitude of the acoustoelectric current density is proportional to $(q\tau)^{-1}/[(v - w)^2 + (q\tau)^{-2}]$, where q is the SAW wavenumber and v the electron velocity. τ is the momentum relaxation time from upper subbands to lower ones. It turned out that τ has mainly two contributions ($\tau^{-1} = \tau_1^{-1} + \tau_2^{-1}$): $\tau_1 \approx L/v$ (wire length L divided by electron velocity) and τ_2 depends on the density of states in the quantum wire. Therefore, the dependence of τ_2 is the main source of the acoustoelectric current oscillation in quantum wires with a strongly oscillating density of states as a function of the energy. Even though this model at present cannot be completely adapted to our experimental findings, it represents, however, an approach to explain the non-monotonic increase of acoustoelectric current. Therefore, in view of future applications we hope to initiate further theoretical work on SAW induced charge transport in GaN quantum wires.

8. Conclusion

In summary, self-organized GaN NWs grown by molecular beam epitaxy on a Si substrate were spread on a piezoelectric host material. The NWs were aligned by the use of a SAW and then electrically contacted. SAWs of different frequencies

were generated in the region of the contacted GaN NWs, and the resulting acoustoelectric DC current was measured as a function of SAW power and frequency. Even though the general dependence of induced acoustoelectric charge transport on SAW amplitude can be explained by the Weinreich equation, the interpretation of a non-monotonic increase of the current at high frequencies and correspondingly short wavelengths comparable to the NW length requires further experimental investigations and theoretical models.

Acknowledgments

Financial support of the German Excellence Initiative via the 'Nanosystems Initiative Munich (NIM)' is gratefully acknowledged.

References

Björk M T, Ohlsson B J, Thelander C, Persson A I, Deppert K, Wallenberg L R and Samuelson L 2002 *Appl. Phys. Lett.* **81** 4458

Bordui P F, Jundt D H, Standifer E M, Norwood R G, Sawin R L and Galipeau J D 1999 *J. Appl. Phys.* **85** 3766

Calarco R, Marso M, Richter T, Aykanat A I, Meijers R, Hart A v d, Stoica T and Lüth H 2005 *Nano Lett.* **5** 981

Cavallini A, Polenta L, Rossi M, Richter T, Marso M, Meijers R, Calarco R and Lüth H 2006 *Nano Lett.* **6** 1548

Cavallini A, Polenta L, Rossi M, Stoica T, Calarco R, Meijers R J, Richter T and Lüth H 2007 *Nano Lett.* **7** 2166

Greytak A B, Lauhon L J, Gudiksen M S and Lieber C M 2004 *Appl. Phys. Lett.* **84** 4176

Gurevich V L, Kozub V I and Pevzner V B 1998 *Phys. Rev.* B **58** 13088

Hoskins M J, Morkoc H and Hunsinger B J 1982 *Appl. Phys. Lett.* **41** 332

Huang Y, Duan X, Cui Y and Lieber C M 2002 *Nano Lett.* **2** 101

Hwang J S, Ahn D, Hong S H, Kim H K, Hwang S H, Jeon B-H and Choi J-H 2004 *Appl. Phys. Lett.* **85** 1636

Meijers R 2006 *J. Cryst. Growth* **289** 381

Motayed A, Davydov A V, Vaudin M D, Levin I, Melngailis J and Mohammad S N 2006 *J. Appl. Phys.* **100** 024306

Rotter M, Kalameitsev A V, Govorov A O, Ruile W and Wixforth A 1999 *Phys. Rev. Lett.* **82** 2171

Rotter M, Ruile W, Bernklau D, Riechert H and Wixforth A 1998 *Appl. Phys. Lett.* **73** 2128

Schmukler B and Hoskins M J 1988 *Appl. Phys. Lett.* **52** 428

Shilton J M, Mace D R, Talyanskii V I, Galperin Y, Simmons M Y, Pepper M and Ritchie D A 1996 *J. Phys.: Condens. Matter* **8** L337

Strobl C J, Schäflein C, Beierlein U, Ebbecke J and Wixforth A 2004 *Appl. Phys. Lett.* **85** 1427

Talyanskii V I, Shilton J M, Pepper M, Smith C G, Ford C J B, Linfield E H, Ritchie D A and Jones G A C 1997 *Phys. Rev.* B **56** 15180

Thelander C, Martensson T, Björk M, Ohlsson B, Larsson M, Wallenberg L and Samuelson L 2003 *Appl. Phys. Lett.* **83** 2052

Weinreich G 1956 *Phys. Rev.* **104** 321

Zhong Z, Wang D, Cui Y, Bockrath M and Lieber C M 2003 *Science* **302** 1377